Journal of Crystal Growth 380 (2013) 228–235

Contents lists available at SciVerse ScienceDirect

Journal of Crystal Growth

journal homepage: www.elsevier.com/locate/jcrysgro

Crystal growth, structural, crystalline perfection, optical and mechanical properties of Nd^{3+} doped sulfamic acid (SA) single crystals

Mohd. Shkir [a,b,c,*], B. Riscob [c], V. Ganesh [e], N. Vijayan [c], Rahul Gupta [d], J.L. Plaza [a], E. Dieguez [a], G. Bhagavannarayana [c]

[a] Crystal Growth Lab, Departamento de Física de Materiales, Universidad Autónoma de Madrid, Madrid 28049, Spain
[b] Advanced Materials Research Lab (AMRL), Department of Physics, Atma Ram Sanatan Dharma (ARSD) College, University of Delhi, New Delhi 110021, India
[c] CSIR-National Physical Laboratory, New Delhi 110012, India
[d] Bruker AXS Analytical Instruments Pvt. Ltd., New Delhi 110019, India
[e] Department of Physics, Kakatiya University, Warangal 506009, India

ARTICLE INFO

Article history:
Received 16 April 2013
Received in revised form
17 June 2013
Accepted 19 June 2013
Communicated by: V. Fratello
Available online 2 July 2013

Keywords:
A. High resolution X-ray diffraction
A2. Growth from solutions
A2. Single crystal growth
B1. Inorganic compounds

ABSTRACT

Sulfamic acid (SA) single crystals, both pure and doped with 1, 2.5 and 5 mol% Nd, were grown successfully in an aqueous solution by the slow cooling method. Powder X-ray diffraction patterns were recorded to check the variation in the lattice parameters and phase of the crystals. The optical transparency was found to be hig Prod. Type: FTPhest (~80%) for the 1 mol% Nd^{3+} doped SA single crystal. The optical band gap was also calculated and found to be ~4.31, 4.20 and 3.67 eV. The influence of Nd^{3+} doping on the crystalline perfection was assessed by a high resolution X-ray diffractometer (HRXRD) and shows that the grown crystals could accommodate Nd^{3+} at the interstitial positions in the crystalline matrix of SA up to some critical concentration without any deterioration in the crystalline perfection. The etching studies were carried out and the etch pits densities were calculated. The mechanical property of grown single crystals was also studied.

1. Introduction

In the recent past the use of optical single crystals has been increased due to their wide application in the field of photonics such as high-speed information processing, frequency conversion, optical communication, high optical disk data storage etc. [1–5]. Due to these challenging applications the growth of single crystals of optical materials is very important for the fabrication of technologically important devices. The use of single crystals is clearly noticeable in industries like electronics and optics. Sulfamic acid (H_3NSO_3) (SA) is the monoamide of sulfuric acid has an orthorhombic structure and the properties of this materials do not change for many years. It is a strong inorganic acid and exhibits zwitterionic form when mixing with water. SA finds good applications in multi stage flash evaporation (MSF) desalination plants for cleaning demisters, heat exchangers, cooling water systems etc. Recently in Japan the industries have established this reagent as a standard substance for titrimetric investigations.

From an application point of view the great effort has been made for the growth and characterization of pure and doped crystals, as the dopants or additives play a vital role in enhancing their physical properties. The concentration of the dopants affects various properties such as: crystalline perfection, optical, mechanical, dielectric, nonlinear etc. [6,7]. Few reports are available on the growth of pure and doped SA crystals by solution and the Sanakaranarayana–Ramasamy (SR) method [8–16].

As per the authors knowledge and available literature there is no report available on the growth and characterization of Nd^{3+} doped SA single crystals. The main aim of the present communication is to study the effect of Nd^{3+} doping on the growth, structural, optical, crystalline perfection and mechanical properties of SA single crystals.

2. Experimental

2.1. Crystal growth

Commercially available 99.99% pure sulfamic acid was used and recrystallized for further purification and then used for single crystal growth by the slow cooling method. Initially a ~1000 ml solution of high homogeneity was prepared for crystal growth according to the solubility of material at 308 K by continuous stirring for more

* Corresponding author at: Advanced Materials Research Lab (AMRL), Department of Physics, Atma Ram Sanatan Dharma (ARSD) College, University of Delhi, New Delhi 110021, India. Tel.: +91 9911769335; fax: +91 1124111390.
E-mail addresses: shkirphysics@gmail.com, shkirarsd.du@gmail.com (Mohd. Shkir).

0022-0248/$ - see front matter © 2013 Elsevier B.V. All rights reserved.
http://dx.doi.org/10.1016/j.jcrysgro.2013.06.022

than 24 h. The prepared solution was filtered in four highly cleaned beakers, from which one was kept as pure covered with a perforated plastic sheet and housed in constant temperature bath.

In the other three beakers neodymium (Nd^{3+}) was added with 1, 2.5 and 5 mol% concentrations and again saturated solutions were prepared in double distilled water at the same temperature with constant stirring for 24 h. The prepared solutions were again filtered in another three beakers, covered with the perforated plastic sheet and then housed in constant temperature bath controlled by a Eurotherm controller at 308 K for crystal growth. After two days we started to reduce the temperature by 1 °C/day and continuously watched with the help of a microscope to observe nucleation. After four days the first nucleation was observed at 304 K and left to grow, but after three days we observed that the growth was very slow. Then we started to reduce the temperature further down to 300 K and observed that the growth rate was increased. We left it for further growth at the same temperature. After 20 days good quality single crystals of hexagonal shape with different morphologies were harvested from the mother solution as shown in Fig. 1.

From the figure it is clear that some growth faces of SA crystals were suppressed and elongated, which may be due to the influence of dopants on the growth of embryos and on the metastable zone width [17]. Also by the addition of metal ions it was found to reduce the effect of impurities to a great extent and hence improve the quality of the crystal surfaces. The presence of impurities is found to have a strong influence on the growth rate, crystalline perfection and many other physical properties.

2.2. Characterizations

Good quality single crystals of pure and Nd^{3+} doped SA were used to prepare fine powders and were filtered using a standard sieve with ~125 MICS aperture openings to a get homogeneous particle size. These powdered specimens were loaded in to the circular sample holder and investigated with a BRUKER D8 ADVANCE powder X-ray diffractometer (PXRD) with CuK_α radiation at a scan rate of 0.02° over the angular range of 5–70° at room temperature. All the parameters of the XRD system were kept same for all the specimens.

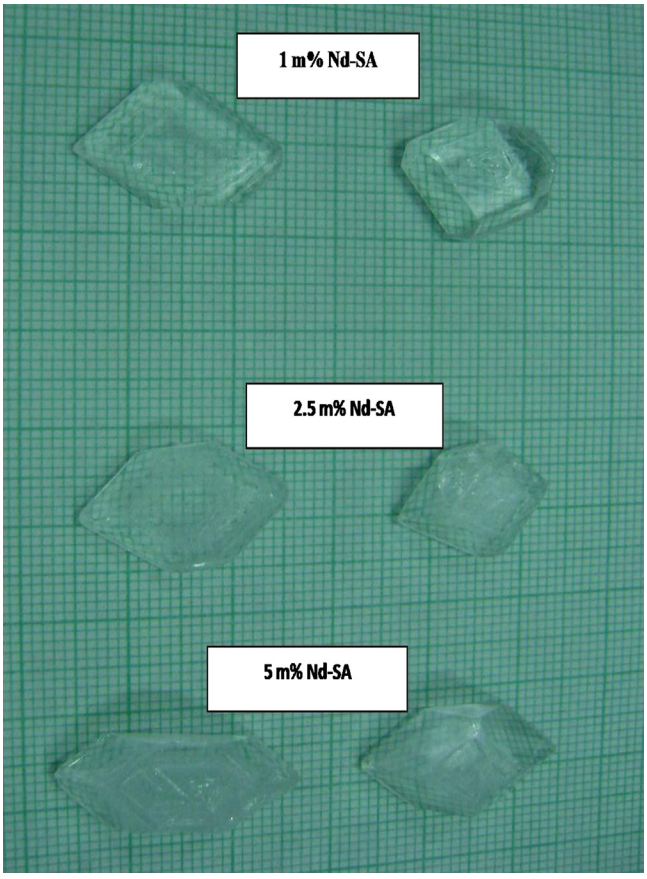

Fig. 1. Photograph of the as-grown Nd^{3+} doped SA single crystals.

Optical transmission spectra of pure and Nd^{3+} doped SA single crystals (thickness ~1.5 mm) were recorded on a prominent (002) face using a Perkin-Elmer Lambda 25 UV–vis spectrophotometer in the wavelength region 200–900 nm at ambient temperature. The recorded data was used to calculate the optical band gaps of the grown crystals.

High-resolution X-ray diffraction (HRXRD) analysis was carried out to evaluate the crystalline perfection of the specimen crystals. A multicrystal X-ray diffractometer developed at the National Physical Laboratory (NPL), New Delhi [18] was used to record high-resolution rocking or diffraction curves (DCs). In this system, a fine focus (0.4×8 mm^2; 2 kW Mo) X-ray source energized by a well-stabilized Philips X-ray generator (PW 1743) was employed. The well-collimated and monochromated $MoK\alpha_1$ beam obtained from the three Si monochromator crystals set in dispersive $(+,-,-)$ configuration has been used as the exploring X-ray beam. This arrangement improves the spectral purity ($\Delta\lambda/\lambda < 10^{-5}$) of the $MoK\alpha_1$ beam. The divergence of the exploring beam in the horizontal plane (plane of diffraction) was estimated to be $\ll 3''$. The specimen crystal is aligned in the $(+,-,-,+)$ configuration. Due to the dispersive configuration of the third monochromator crystal with respect to the 2nd monochromator, the spectral quality of the diffracted beam emerging from the 3rd third monochromator has a high degree of perfection and hence, though the lattice constant of the monochromator crystal and the specimen are different, the unwanted experimental dispersion broadening in the diffraction curve of the specimen crystal [ΔFWHM$=$ $\Delta\lambda/\lambda(\tan\theta_M - \tan\theta_S)$; where θ_M and θ_S are the Bragg diffraction angles of the monochromator and specimen crystals] is insignificant. The advantage of the dispersion configuration $(+,-,-)$ over the non-dispersive configuration $(+,-,+)$ of monochromators is well described in our recent article [19]. The specimen can be rotated about a vertical axis, which is perpendicular to the plane of diffraction, with a minimum angular interval of 0.4″. The diffracted intensity is measured using a scintillation counter. The DCs were recorded by changing the glancing angle (angle between the incident X-ray beam and the surface of the specimen) around the Bragg diffraction peak position θ_B (taken zero as reference point) starting from a suitable arbitrary glancing angle (θ). The detector was kept at the same angular position $2\theta_B$ with wide opening for its slit, the so-called ω scan [19]. The omega scan is very appropriate to record the short range order scattering caused by defects, by scattering from local Bragg diffractions from agglomerated point defects or due to low angle and very low angle structural grain boundaries [20].

Vickers microhardness studies were carried out using a Leitz–Wetzlar hardness tester equipped with a diamond square indenter. Different loads ranging from 10 to 100 g were used for these studies with a constant indentation time of 10 sec for all these crystals. The distance between any two consecutive indentations is kept at more than five times the diagonal length of the indention mark in order to avoid surface effects. For the hardness studies, the crystals are ground with SiC paper down to 600grit and then polished with methanol solution to remove the surface damages. The indentations were made with a Vickers Microhardness tester. At least five indentations were made on the face of pure and Nd^{3+} doped SA single crystals at every load. The average diagonal length of the indentation impression at each load was used for measuring the microhardness value (H_v). The mechanical

contact between the indenter and the crystal surface produces radial cracks. So, the fracture toughness value (K_c) which is another mechanical parameter, was determined by measuring the crack lengths of radial cracks.

3. Results and discussion

3.1. Powder X-ray diffraction analysis

The powder XRD pattern of pure as well as Nd^{3+} doped SA single crystals were recorded as shown in Fig. 2, and found to contain all the original peaks of SA [10]. The observed 2 theta and *d* values for the doped SA crystals are given in Table 1. The recorded data was used to calculate lattice parameters using POWDERX and CHECKCELL software from which it was confirmed that the grown crystals belong to the orthorhombic system with the non-centrosymmetric space group *Pbca*. The hkl, 2 theta and *d* values of Nd^{3+} doped SA single crystals are presented in Table 1 and the calculated lattice parameters are given in Table 2 and found to be in good agreement with the earlier reported values [11,16]. No new phase was observed except a minute variation in the angular values in the XRD pattern that may be due to incorporation of dopants leading to a slight variation in lattice parameters of the grown crystals. From Fig. 2 it is also clear that

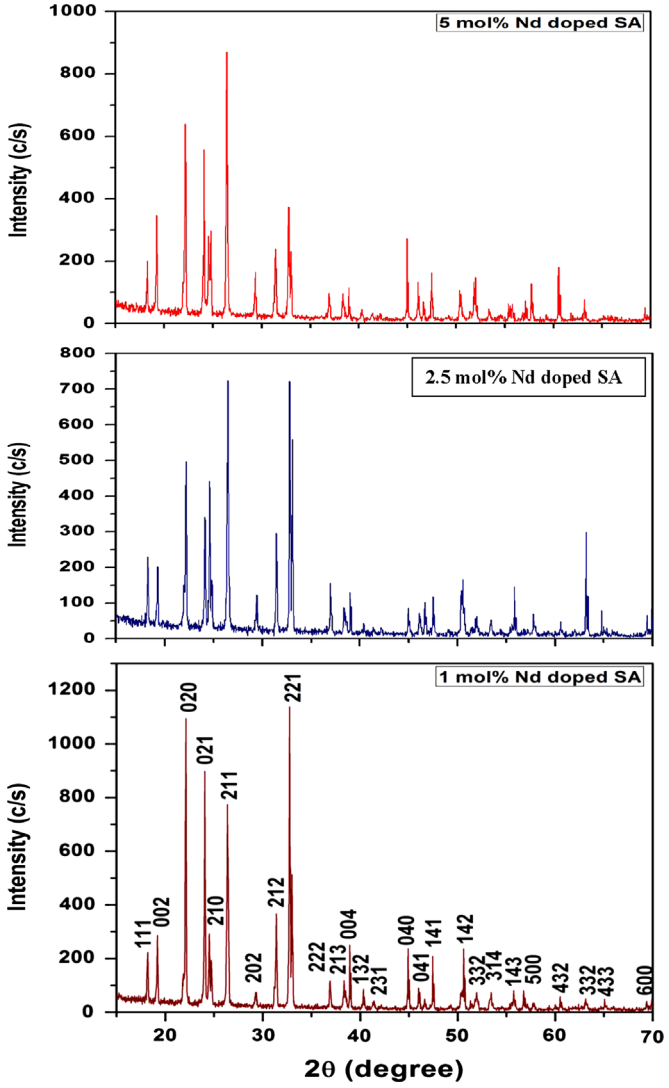

Fig. 2. XRD pattern of pure and Nd^{3+} doped SA crystals.

Table 1
The hkl, 2 theta and *d* values of Nd^{3+} doped SA single crystals.

Planes	1 mol% Nd^{3+} doped SA		2.5 mol% Nd^{3+} doped SA		5 mol% Nd^{3+} doped SA	
hkl	2θ (deg)	*d* (Å)	2θ (deg)	*d* (Å)	2θ (deg)	*d* (Å)
111	18.203	4.86958	18.252	4.85655	18.245	4.85861
2	19.198	4.61951	19.263	4.60395	19.212	4.61601
20	22.114	4.01653	23.468	3.7877	21.119	4.20331
21	24.059	3.69603	24.109	3.68845	24.076	3.69338
210	24.588	3.61764	24.588	3.61764	24.803	3.58683
211	26.378	3.37608	26.453	3.36666	26.401	3.37319
202	29.346	3.04107	29.426	3.03295	29.365	3.03909
212	31.396	2.84698	31.445	2.84263	31.446	2.8426
221	32.757	2.73178	32.79	2.7291	32.782	2.72968
23	36.904	2.43374	36.98	2.4289	36.153	2.48255
213	38.342	2.34568	38.359	2.3447	38.347	2.3454
4	38.924	2.31195	38.987	2.30837	38.967	2.30952
132	40.316	2.2353	40.396	2.23101	40.306	2.23582
231	41.412	2.17859	41.345	2.18199	41.431	2.17765
40	44.907	2.01683	44.968	2.01423	44.942	2.01534
401	45.976	1.97239	46.062	1.96892	46.055	1.96919
124	46.61	1.94704	46.65	1.94546	46.626	1.94639
141	47.437	1.91501	47.489	1.91303	47.464	1.91397
142	50.614	1.80201	50.554	1.80401	50.354	1.81068
332	51.922	1.75963	51.996	1.7573	51.992	1.75743
314	53.44	1.71318	53.477	1.71209	53.342	1.7161
143	55.744	1.64771	55.842	1.64506	55.359	1.65825
430	56.765	1.62047	56.792	1.61978	57.131	1.61097
432	60.509	1.52886	60.573	1.52738	60.535	1.52826
334	63.121	1.47173	63.182	1.47045	63.183	1.47042
433	65.078	1.43212	65.856	1.41706	65.166	1.43039

Table 2
Lattice parameters of pure and Nd^{3+} doped SA single crystals.

Sample	*a* (Å)	*b* (Å)	*c* (Å)	*V* (Å^3)
Pure SA [11,16]	8.078/8.0660	8.116/8.1150	9.268/9.2550	607.62/605.791
Pure SA [16]	8.115	8.066	9.255	602.221
1.0 mol% NDSA	8.1174	8.0654	9.222	603.764
2.5 mol% NDSA	8.1105	8.0593	9.2202	602.679
5.0 mol% NDSA	8.109	8.0622	9.2301	603.431

the intensity of the peaks for 1 mol% Nd doped SA crystal is higher than for the other doping concentrations and also exceeds all other doping concentrations from an earlier report [10].

3.2. Optical analysis

3.2.1. UV–vis optical transmission analysis

The recorded optical transmission spectrum of Nd^{3+} doped SA single crystal is shown in Fig. 3. It clear from the figure that the optical transparency increased with a Nd^{3+} doping of 1.0 mol% and then gradually decreased for 2.5 and 5.0 mol% doping concentration but still higher than pure and previously studied doped SA single crystals [9–12]. The high transmission in the entire region also confirmed the colorless nature of the grown crystal. Scattering centers were responsible for the optical loss and the improvement of the optical transmittance in 1 Mol% doped NdSA crystal maybe due to the reduction of the scattering centers from crystallographic defects and structural defects [21–23]. The crystal grown with 1.0 mol% doping is good from an applications point of view as its transparency is higher in comparison with other crystals and also has superior PXRD and HRXRD results. Hence the titled compound could be a good candidate for fabrication of optical devices.

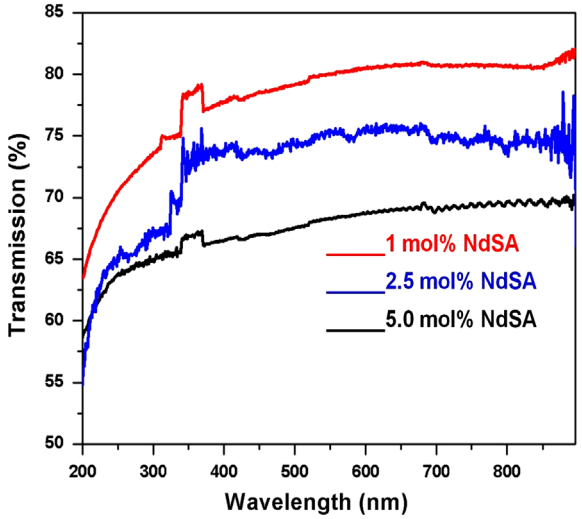

Fig. 3. UV–vis spectra of Nd^{3+} doped SA crystals.

3.2.2. Optical band gap analysis

The recorded data was used to calculate the optical band gap of the grown crystals. First the absorption spectrum was obtained from the transmission data then optical absorption coefficient (α) was calculated using the relation

$$\alpha = \text{Absorption}/t \quad (1)$$

where t is the thickness of the used crystal. The optical band gap (E_g) was calculated from the optical absorption coefficient (α) near the absorption edge from the following relation:

$$\alpha h\nu = A(h\nu - E_g)^{1/2} \quad (2)$$

where A is a constant, E_g is the optical band gap, h is Plank's constant and ν is the frequency of the incident photons. The band gap of the grown crystals was calculated by extrapolating the straight line to the x-axis ($h\nu$) as shown in Fig. 4 and found to be ~4.31, 4.20 and 3.67 eV for 1 mol%, 2.5 mol% and 5 mol% Nd^{3+} doped SA crystals respectively.

3.3. HRXRD analysis

Fig. 5(a) shows the high-resolution diffraction curve (DC) recorded for a 1 mol% Nd-doped SA specimen crystal using the (002) diffracting planes in symmetrical Bragg geometry by employing a multicrystal X-ray diffractometer with MoKα_1 radiation. As seen in the figure the DC is quite sharp without any satellite peaks which may otherwise be observed either due to internal structural grain boundaries [24] or due to an epitaxial or complexing layer that may sometimes form in crystals grown from solution using dopants [25]. The full width at half maximum (FWHM) of the diffraction curves is 4″, which is quite low and close to that expected from the plane wave theory of dynamical X-ray diffraction [26]. The single sharp diffraction curve with very low FWHM indicates that the crystalline perfection is extremely good and also better than the earlier reports on pure and doped SA crystals [9–12]. The specimen is a nearly perfect single crystal without having any internal structural grain boundaries. However, when we compare the scattered intensity along the wings/tails of the curve, for a particular angular deviation ($\Delta\theta$) of glancing angle with respect to the peak position, the scattered intensity is slightly more in the negative direction in comparison to that of the positive direction, which can be seen prominently in Fig. 5(b) as described in the following.

Fig. 5(b) shows the high-resolution diffraction curve for a 2.5 mol% Nd-doped SA single crystal recorded under identical

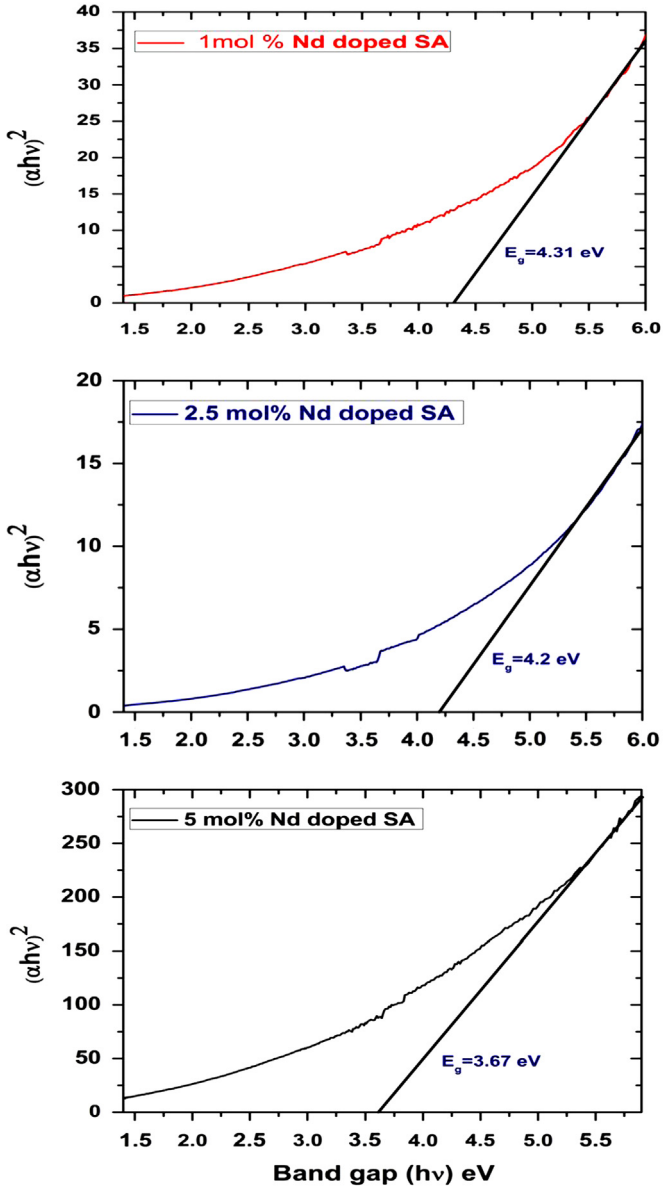

Fig. 4. Optical band gap of 1 mol%, 2.5 mol% and 5 mol% Nd^{3+} doped SA crystals.

experimental conditions including the X-ray beam size (0.2 mm × 5 mm) and intensity (9 kc/s). As seen in the figure, the DC contains a single peak and indicates that the specimen is free from structural grain boundaries. The FWHM (full width at half maximum) of the curve is 18″, which is more than that of curve (a). Just like in Fig. 4(a), it is interesting to see the asymmetry of the DC. For a particular angular deviation ($\Delta\theta$) of the glancing angle with respect to the peak position, the scattered intensity is much more in the negative direction in comparison to that of the positive direction. This feature clearly indicates that the crystal contains predominantly vacancy defects rather than interstitial defects. This can be well understood by the fact that due to vacancy defects, as shown schematically in the inset, the lattice around these defects undergo tensile stress and the lattice parameter and d (interplanar spacing) increase leading to more scattered (also known as diffuse X-ray scattering) intensity at slightly lower Bragg angles (θ_B) as d and sin θ_B are inversely proportional to each other in the Bragg Eq. (2) $d \sin\theta_B = n\lambda$; n and λ being the order of reflection and wavelength respectively, which are fixed. More details may be obtained from the study of high-resolution diffuse X-ray scattering

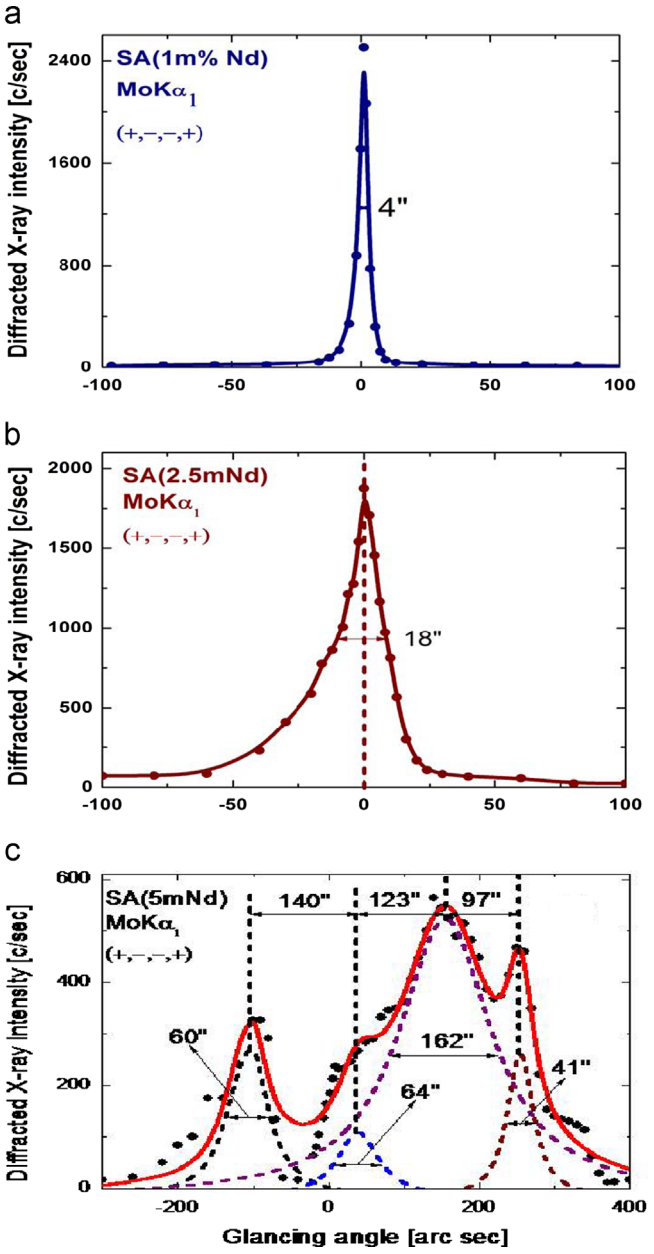

Fig. 5. High-resolution X-ray diffraction curves recorded for (002) diffracting planes of Nd-doped SA single crystals with doping values: (a) 1 mol%, (b) 2.5 mol % and (c) 5 mol%.

measurements [27], which is not the main focus of the present investigation. If the concentration is high, the FWHM would be much higher and often lead to structural grain boundaries [28]. Point defects up to some extent are unavoidable due to thermodynamical considerations. It may be mentioned here that the variation in lattice parameter is confined very close to the defect core, which gives only scattered intensity close to the Bragg peak. Long range order could not be expected and hence a change in the lattice parameter is also not expected [29]. It may be worth mentioning here that the Nd-dopants are more or less statistically distributed in the crystal. If the dopants or impurities are not statistically distributed, but distributed here and there as macroscopic clusters, then the strain generated by such clusters is larger leading to cracks and structural grain boundaries. These can be seen very clearly in HRXRD curves with additional peak(s) as observed in our recent study on urea-doped crystals in ZTS at various levels of doping [19]. The above analysis clearly indicates that the Nd-doped SA contains vacancy defect, it might have replaced K^+ ions leading to vacancy for each Nd incorporated at substitutional sites for charge neutrality. The heavy asymmetry in Fig. 5(b) in comparison with that of Fig. 5(a) indicates the incorporation of more Nd^{3+} in the specimen with 2.5 mol% doping than that of the 1 mol% specimen.

Fig. 5(c) shows the DC recorded for the 5 mol% Nd-doped specimen. The DC is quite different from that of curves (a) and (b) with multiple peaks. The solid line (convoluted curve) is well fitted with the experimental points represented by the filled rectangles. On deconvolution of the diffraction curve, it is clear that the curve contains three additional peaks, which are 140, 123 and 97″ away from their adjoining regions. These three additional peaks correspond to three internal structural low angle boundaries ($>1'$ but less than a degree) [24], whose tilt angles are 140, 123 and 97″ from their adjoining regions. Tilt angle may be defined as the misorientation angle between the two crystalline regions on both sides of the structural grain boundary. The FWHM (full width at half maximum) of the different boundaries are 60, 64, 162 and 41″. These observed boundaries are due to strains developed by the heavy doping of Nd^{3+} which causes antisite defects and associated vacancy defects. Though the specimen contains grain boundaries, the low FWHM values and the low angular spread of around 600″ (one sixth of a degree) of the diffraction curve indicate that the crystalline perfection is fairly good.

3.4. Chemical etching study

To study the defect structure of a single crystal, etching is the simplest characterization technique that can be used. However, the success of this technique lies in the efficiency of the chemical etchant to sense the dislocation sites selectively in the specimen. The etch pits are formed at the dislocation centers on those faces of the grown crystals at which the additives are bound. The chemical etching studies were carried out on Nd^{3+} doped SA single crystals with a number of etchants (ethanol, methanol, acetone, water etc.), but the best etching action was observed with water and the etching time was kept constant (20 s) for all samples. The shape of the etch pits are almost all similar (elongated rectangles) for the present crystals but the etch pit density is different for different concentrations of impurities/dopants. In chemical etching the etching time, concentration of etchant or etchant ratio and selective etchant play vital roles [30]. The ⟨100⟩ faces of grown Nd^{3+} doped SA single crystals were subjected to etching with water at room temperature. Fig. 6(a), (b) and (c), shows the surfaces of the grown crystals of 1, 2.5 and 5 mol% Nd^{3+} doped SA respectively. The etch pit densities were calculated for all the specimen crystals and found to be in the range of 2.2×10^3, 3.4×10^3 and 4.5×10^3. In the present study a lower etch pit density is observed in the case 1.0 mol% Nd^{3+} doped SA crystals showing that the crystals have fewer defects which consistent with HRXRD and UV–vis–NIR studies and thus these crystals can used for optical device fabrication. In utilizing single crystals for applications it is essential to grow single crystals containing a reduced dislocation density [31]. A decrease in etch pit density (EPD) is associated with more systematic packing of the atoms during growth [32] in the 1 mol% Nd^{3+} doped SA crystal.

3.5. Mechanical study

Hardness of the material plays a vital role in device fabrications and their stability. Therefore, it is very important to know the mechanical strength of the crystal before using this material for the fabrication of optical devices. It is a measure of the resistance offered by the lattice to permanent deformation. The indentations were made on the ⟨100⟩ face of the doped crystals. Fig. 7 shows the

indentations made on the face of Nd^{3+} doped SA single crystals. Hardness of all the doped crystals was calculated using the following relation:

$$H_v = 1.854P/d^2 \text{ kg/mm}^2 \quad (3)$$

where H is the Vickers hardness number, P is the indentation load in kilogram and d is the diagonal length of the indentation mark (Fig. 8) in millimeter. The microhardness values were taken as the average of the several impressions made. Hardness values estimated in these samples show a normal trend that as the load increases, the value of the hardness increases with increasing the doping concentration of Nd^{3+} and reaches a load independent region as shown in Fig. 8(a) (Table 3). The strength of the grown crystals is found to be enhanced with Nd^{3+} doping. The hardness of the doped crystals in the present investigation was found to be higher than the pure, SR grown as well as with other dopants in sulfamic acid crystals in previous studies [10–12]. An increase in the mechanical strength will have significant effect on fabrication of devices and processing such as ease of crystal polishing and less wastage due to cracking/breakage while polishing [33–35].

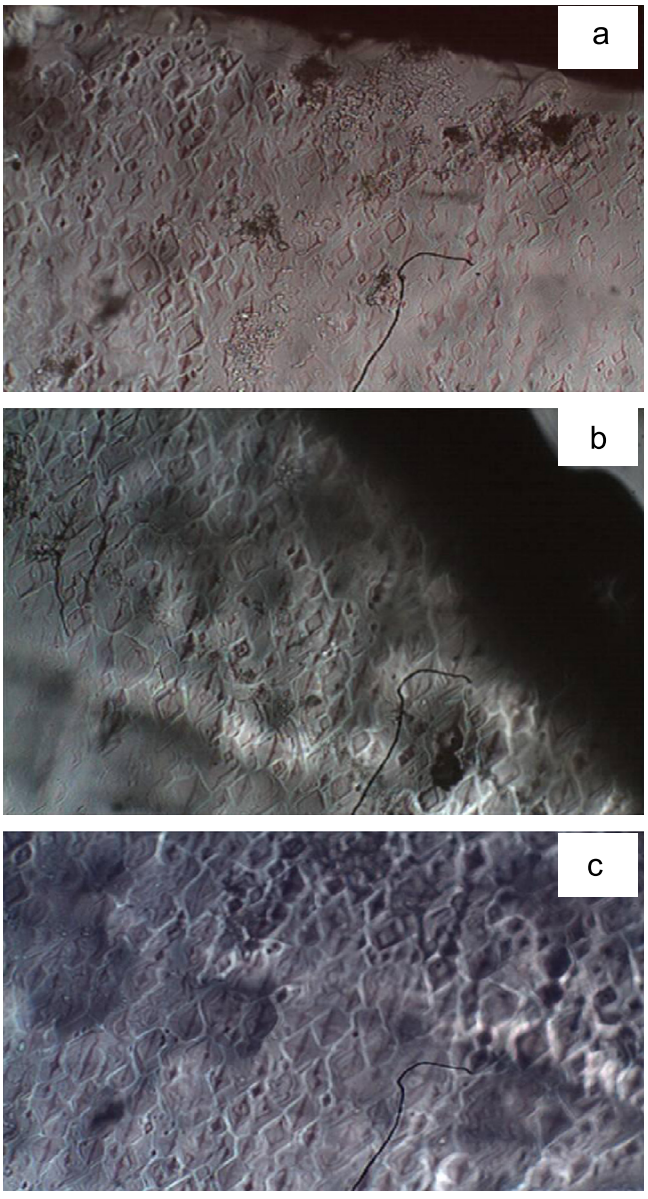

Fig. 6. Etch pit patterns of (a) 1 mol%, (b) 2.5 mol% and (c) 5.0 mol% NdSA single crystals.

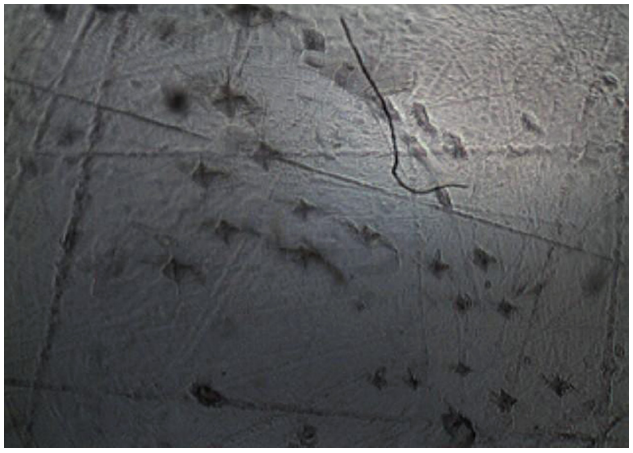

Fig. 7. Vickers indentation mark on doped SA crystal at different loads.

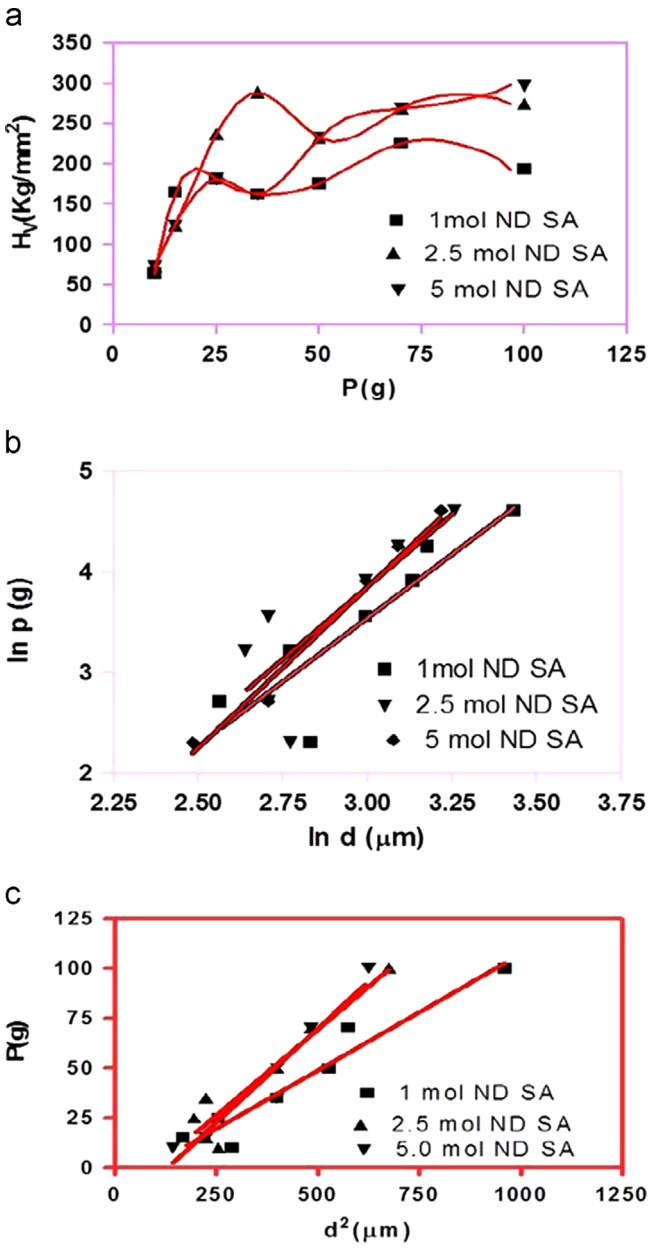

Fig. 8. Plots of variations (a) Vickers hardness H_v with load P, (b) ln P vs. ln d and (c) P vs. d^2 of Nd^{3+} doped SA crystals.

Table 3
Mechanical parameters of Nd^{3+} doped SA crystals.

Crystal	H_v (Kg/mm^2)	n	W (g)	H_o (Kg/mm^2)	K_c (g/μm$^{3/2}$)	B_i (μm$^{-1/2}$)
1.0 mol%	192	1.52	0.1	185.4	0.076	5619.52
2.5 mol%	274	2.02	0.12	222.4	0.082	5576.09
5.0 mol%	296	2.22	0.13	241	0.099	3759.64

Meyer's law is given by following relation:

$$P = K_1 d^n \tag{4}$$

where P is the load applied, d is the diagonal length of impression, K_1 is a constant and n is Meyer's index or work-hardening coefficient. The n value is estimated from the slope of ln P vs. ln d plots shown in Fig. 8(b) and given in Table 2. Onitsch [36] and Hanneman [37] had shown that the value of n comes out to be 1–1.6 for hard materials and more than 1.6 for soft ones.

In the present study the Meyer index number was found to be 1.5, 2.0 and 2.2 for 1, 2.5 and 5 mol% Nd^{3+} doped SA crystals, respectively and clearly indicates that the crystals grown with 1 mol% Nd doping belongs to harder and rest are belongs to soft material category. According to the Hays–Kendall approach [38], the load dependence of the hardness is given by the following relation:

$$P = W + A_1 d^2 \tag{5}$$

where, W is the minimum load to initiate plastic deformation and A_1 is a load independent constant. These two values were calculated from the plot drawn between P vs. d^2 shown in Fig. 8 (c), where W is the intercept along the load axis and A_1 is the slope. The corrected hardness H_o for Nd^{3+} doped crystals was calculated by using the following relation:

$$H_o = 1854 A_1 \tag{6}$$

The n, W and H_o values for Nd^{3+} doped SA single crystals are given in Table 3.

3.5.1. Fracture toughness, Brittle index

The resistance to fracture indicates the toughness of any material. Fracture toughness (K_c) determines how much fracture stress is applied under uniform loading and is an important parameter for the selection of materials for device applications where the load exceeds the limit or yield point [39]. Fracture toughness provides the most reasonable estimation of the fracture resistance of brittle materials. There are two modeling approaches to crack systems that can be developed in a material as a result of indentations. Those crack systems are radial–median and Palmqvist crack systems. The crack lengths (c) were measured from centers of the indentation to tip of the crack. The crack length bears a linear relationship with applied load as shown in Fig. 9(a). When $c/a \geq 2.5$ (a being the half diagonal length of the indentation mark$=d/2$), the cracks developed are median and the fracture toughness, K_c is calculated using the following relation [40]:

$$K_c = kP/c^{3/2} \tag{7}$$

where, k ($=1/7$) is a constant for Vickers indenter [41]. When $c/a \leq 2.5$ the cracks formed during indentation have the configuration of Palmqvist cracks and the fracture toughness may be calculated using the following relation [42,43]:

$$K_c = kP/al^{1/2} \tag{8}$$

where $l = c - a$, is the mean Palmqvist crack length.

Eq. (8) was used to calculate the fracture toughness K_c. The fracture toughness of the material which shows the resistance to fracture also increases with doping concentration as shown in Fig. 9(b) and the values are given in Table 3.

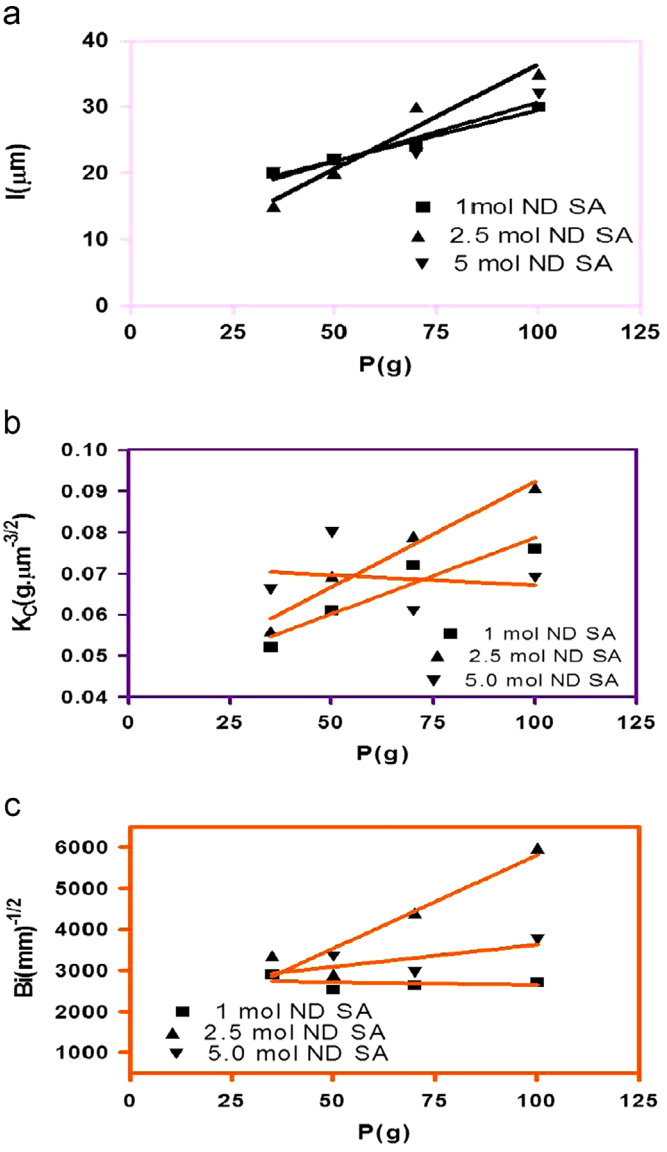

Fig. 9. Plots of variations (a) crack length l with load P, (b) fracture toughness K_c with load P and (c) brittle index number B_i with load P of Nd^{3+} doped SA crystals.

The brittleness is a key property of the single crystals which determines its fracture without any appreciable deformation. It is expressed in terms of the brittleness index (B_i) and is estimated using the following relation [44]:

$$B_i = H_v/K_c \tag{9}$$

The variations of brittleness index with load for 1, 2.5 and 5 mol % Nd^{3+} doped SA crystals are shown in Fig. 9(c). Figure shows that the Brittle index number is decreases with doping concentration [Table 3].

4. Conclusions

Good quality single crystals of SA were grown with different doping concentrations of Nd^{3+}. The crystal system and lattice parameters were confirmed and calculated, which reveals that the doping does not affect the crystal system as well as lattice parameters. The enhancement of percentage of transmission in

the recorded UV–vis–NIR region indicates that optical damage can be reduced by Nd^{3+} doping. The optical transparency in 1 mol% NdSA was found to be higher than other doping concentrations. HRXRD studies show that the grown crystals could accommodate Nd^{3+} at the interstitial positions in the crystalline matrix of SA up to some critical concentration without any deterioration in the crystalline perfection. The etching studies also show that the 1 mol % NdSA crystals are more perfect than the other crystals. The mechanical strength was also found to increase with Nd^{3+} doping. From the above studies it is clear that Nd^{3+} doped SA crystals can be a good engineering material for optical device applications.

Acknowledgment

Author Dr. Mohd. Shkir (Shakir) is highly thankful to the Principal (Dr. S.K. Sharma) and Teaching Incharge, Department of Physics (Dr. Nutan Mishra), ARSD College, University of Delhi for their kind support.

References

[1] B.E.A. Saleh, M.C. Teich, Fundamental of Photonics, Wiley, New York, 1991.
[2] B.G. Penn, B.H. Cardelino, C.E. Moore, A.W. Shields, D.O. Frazier, Progress in Crystal Growth and Characterization 22 (1991) 19–51.
[3] D.J. Williams, Angewandte Chemie International Edition in English 23 (1984) 690–703.
[4] N.P. Zaitseva, L. Carman, Progress in Crystal Growth and Characterization 43 (2001) 1–118.
[5] J. Badan, R. Hierle, A. Perigaud, J. Zyss, NLO properties of Organic Molecules and Polymeric Materials, in: D.J. Williams (Ed.), American Chemical Symposium Series 233, American Chemical Society, Washington, DC, 1993.
[6] S.K. Kushwaha, Mohd. Shakir, K.K. Maurya, A.L. Shah, M.A. Wahab, G. Bhagavannarayana, Journal of Applied Physics 108 (2010) 033506–033507.
[7] Mohd. Shakir, V. Ganesh, M.A. Wahab, G. Bhagavannarayana, K. Kishan Rao, Materials Science and Engineering B 172 (2010) 9–14.
[8] H.L. Bhat, Progress in Crystal Growth and Characterization 11 (1985) 57–87.
[9] M.Senthil Pandian, Urit Charoen In, P. Ramasamy, Prapun Manyum, M. Lenin, N. Balamurugan, Journal of Crystal Growth 312 (2010) 397–401.
[10] R. Ramesh Babu, R. Ramesh, R. Gopalakrishnan, K. Ramamurthi, G. Bhagavannarayana, Spectrochimica Acta Part A 76 (2010) 470–475.
[11] T. Thaila, S. Kumararaman, Spectrochimica Acta Part A 82 (2011) 20–24.
[12] R. Valluvan, K. Selvaraju, S. Kumararaman, Materials Chemistry and Physics 97 (2006) 81–84.
[13] S.J. Hickling, R.G. Woolley, Chemical Physics Letters 166 (1990) 43–48.
[14] G. Lucazeau, A. Lautie, A. Novak, Journal of Raman Spectroscopy 3 (1975) 161–165.
[15] T. Yoshimori, T. Tanaka, Analytica Chimica Acta 66 (1973) 85–91.
[16] R.L. Sass, Acta Crystallographica 13 (1960) 320–324.
[17] S. Titiz-Sargut, J. Ulrich, Crystal Growth and Design 2 (2002) 371–374.
[18] K. Lal, G. Bhagavannarayana, Journal of Applied Crystallography 22 (1989) 209–215.
[19] G. Bhagavannarayana, S.K. Kushwaha, Journal of Applied Crystallography 43 (2010) 154–162.
[20] K. Senthilkumar, S. Moorthy Babu, G. Bhagavannarayana, Journal of Applied Crystallography 44 (2011) 313–318.
[21] Yaoshui Wang, Manna Zheng, P. Bennema, Rui Zhu, Guifen Ye, Xiangyang Liu, W.J.P. van Enckevort, Journal of Crystal Growth 108 (1991) 821–826.
[22] M. Senthil Pandian, K. Boopathi, P. Ramasamy, G. Bhagavannarayana, Materials Research Bulletin 47 (2012) 826–835.
[23] M. Senthil Pandian, N. Pattanaboonmee, P. Ramasamy, P. Manyum, Journal of Crystal Growth 314 (2011) 207–212.
[24] G. Bhagavannarayana, R.V. Ananthamurthy, G.C. Budakoti, B. Kumar, K.S. Bartwal, Journal of Applied Crystallography 38 (2005) 768–771.
[25] G. Bhagavannarayana, S. Parthiban, Subbiah Meenakshisundaram, Journal of Applied Crystallography 39 (2006) 784–790.
[26] B.W. Betterman, H. Cole, Reviews of Modern Physics 36 (1964) 681–717.
[27] G. Bhagavannarayana, S. Parthiban, Subbiah Meenakshisundaram, Crystal Growth and Design 8 (2008) 446–451.
[28] G. Bhagavannarayana, A. Choubey, Yu.V. Shubin, Krishan Lal, Journal of Applied Crystallography 38 (2005) 448–454.
[29] G. Bhagavannarayana, S.K. Kushwaha, Mohd. Shakir, K.K. Maurya, Journal of Applied Crystallography 44 (2010) 122–128.
[30] K. Sangwal, Etching of Crystals, North Holland Physics Publishing, Amsterdam, The Netharlands, 1987.
[31] M. Senthil Pandian, N. Balamurugan, G. Bhagavannarayana, P. Ramasamy, Journal of Crystal Growth 310 (2008) 4143–4147.
[32] M. Senthil Pandian, P. Ramasamy, Binay Kumar, Materials Research Bulletin 47 (2012) 1587–1597.
[33] M. Senthil Pandian, P. Ramasamy, Materials Chemistry and Physics 132 (2012) 1019–1028.
[34] M. Senthil Pandian, P. Ramasamy, Journal of Crystal Growth 312 (2010) 413–419.
[35] M. Senthil Pandian, N. Balamurugan, V. Ganesh, P.V. Raja Shekar, K. Kishan Rao, P. Ramasamy, Materials Letters 62 (2008) 3830–3832.
[36] E.M. Onitsch, Mikroskopia 2 (1947) 131–135.
[37] M. Hanneman, Metall, Manch 23 (1941) 135–140.
[38] C. Hays, E.G. Kendall, Metallography 6 (1973) 275–282.
[39] V. Gupta, K.K. Bamzai, P.N. Kotru, B.M. Wanklyn, Materials Chemistry and Physics 89 (2005) 64–71.
[40] A. Jain, A.K. Razdan, P.N. Kortu, B.M. Wankyln, Journal of Materials Science 29 (1994) 3847–3856.
[41] B.R. Lawn, E.R. Fuller, Journal of Materials Science 10 (1975) 2016–2020.
[42] P. Mythili, T. Kanagasekaran, R.Gopala Krishnan, Crystal Research and Technology 42 (2007) 791–799.
[43] Mohd. Shkir, V. Ganesh, N. Vijayan, B. Riscob, Anoop Kumar, Devendra Kumar Rana, Mohd. Hasmuddin, M.A. Wahab, R. Ramesh babu, G. Bhagavannarayana, Spectrochimica Acta A 103 (2013) 199–204.
[44] D. Townsend, J.E. Field, Journal of Materials Science 25 (1990) 1347–1352.